RSC Advances

PAPER

View Article Online
View Journal | View Issue

Cite this: *RSC Adv.*, 2021, **11**, 27674

The molecular mechanism of P450-catalyzed amination of the pyrrolidine derivative of lidocaine: insights from multiscale simulations†

Conger Wang, Peng Wu, Zhanfeng Wang and Binju Wang *

Nitrogen heterocycles are key and prevalent motifs in drugs. Evolved variants of cytochrome $P450_{BM3}$ (CYP102A1) from *Bacillus megaterium* employ high-valent oxo-iron(IV) species to catalyze the synthesis of imidazolidine-4-ones *via* an intramolecular C–H amination. Herein, we use multi-scale simulations, including classical molecular dynamics (MD) simulations, quantum mechanical/molecular mechanical (QM/MM) calculations and QM calculations, to reveal the molecular mechanism of the intramolecular C–H amination of the pyrrolidine derivative of lidocaine bearing cyclic amino moieties catalyzed by the variant RP/FV/EV of $P450_{BM3}$, which bears five mutations compared to wild type. Our calculations show that overall catalysis includes both the enzymatic transformation in P450 and non-enzymatic transformation in water solution. The enzymatic transformation involves the exclusive hydroxylation of the C–H bond of the pyrrolidine derivative of lidocaine, leading to the hydroxylated intermediate, during which the substrate radical would be bypassed. The following dehydration and C–N coupling reactions are found to be much favored in aqueous situation compared to that in the non-polar protein environment. The present findings expand our understanding of the P450-catalyzed C(sp_3)–H amination reaction.

Received 12th June 2021
Accepted 9th August 2021

DOI: 10.1039/d1ra04564d

rsc.li/rsc-advances

1. Introduction

Nitrogen heterocycles constitute one of the most prevalent motifs in drugs.[1] As such, numerous chemical approaches have been developed for the intra- and inter-molecular C–H aminations. Among these approaches, the biosynthesis of C–N bonds using enzymes represents an attractive approach concerning their benign conditions. As a versatile biocatalyst, cytochrome P450 can catalyse a wide range of reactions, such as hydroxylation, epoxidation, reductive dehalogenation, amine dealkylation and sulfoxidation.[2] The coupled high-valent oxo-iron(IV) porphyrin π-radical cation species, so called compound I (**Cpd I**), has been well recognized as the principal oxidant of P450.[2–9] Utilizing organic azides as the nitrene precursor, Fasan and co-workers found that cytochrome P450 could catalyse the intramolecular C–H amination of sulfonyl azides *via* the nitrene transfer reactions.[10,11] In a subsequent work, Arnold and co-workers successfully engineered P450 to obtain the highly enantioselective intermolecular amination of benzylic C–H bonds.[12]

In addition to the nitrene transfer reactions using organic azides, Wong and co-workers found the P450-mediated metabolite of the pyrrolidine derivative of lidocaine led to an unusual cyclization product,[13] which is expected to be generated *via* a P450-**Cpd I** mediated intramolecular C–H amination. The following work by Wong and co-workers expand the similar reaction to a biosynthesis of a wide array of imidazolidin-4-ones using the evolved variants of cytochrome $P450_{BM3}$, which may have potential bioactivity.[14] Unlike the nitrene transfer reactions, P450-**Cpd I** mediated intramolecular C–H amination utilizes the common aminoacetamide as a substrate, which is easily available. Notably, a few P450 oxidases have been discovered to catalyse the intra- or inter-molecular C–N bond-forming reactions in recent studies.[15–20] It was suggested[14] that the reaction is initiated by the **Cpd I**-mediated H-atom abstraction (HAA) from the pyrrolidine derivative of lidocaine, leading to substrate radical and Fe(IV)–OH intermediate (Scheme 1). Next, two plausible mechanisms were proposed for P450-catalyzed amination of the pyrrolidine derivative of lidocaine. In the mechanistic route I, the one-electron oxidation of the pyrrolidine derivative of lidocaine by **Cpd I** may first lead to the iminium species, which may further undergo the intramolecular cyclization to form the *N*,*N*-acetal. In the alternative route II, the substrate radical may undergo a OH rebound reaction to afford the hydroxylated pyrrolidine derivative of lidocaine, which may further lose the hydroxide to form an iminium ion. Although the P450-**Cpd I** mediated intramolecular

State Key Laboratory of Physical Chemistry of Solid Surface, Fujian Provincial Key Laboratory of Theoretical and Computational Chemistry, College of Chemistry and Chemical Engineering, Xiamen University, Xiamen 361005, P. R. China. E-mail: wangbinju2018@xmu.edu.cn

† Electronic supplementary information (ESI) available. See DOI: 10.1039/d1ra04564d

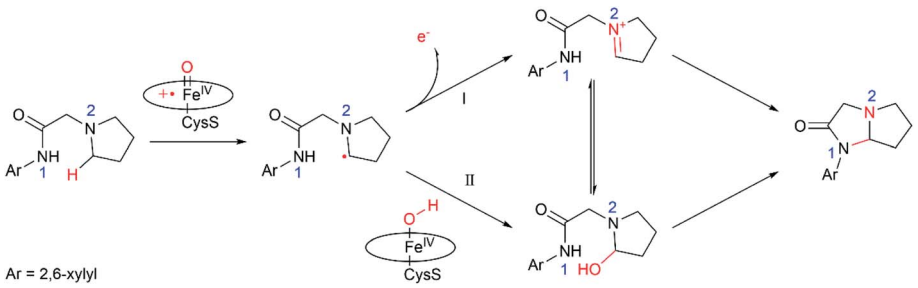

Scheme 1 Two possible mechanisms proposed in ref. 12.

C–H amination is promising in the synthesis of imidazolidin-4-ones, the detailed mechanism of these processes is still unclear. For instance, how does P450 selectively oxidize the α-site C–H without oxidizing other C–H or N1–H bonds? Which mechanistic pathway is more favourable, route I or II? How is the intramolecular cyclization completed, enzymatic or non-enzymatic?

To solve above issues, the combined molecular dynamics (MD) simulations, quantum mechanical/molecular mechanical (QM/MM) calculations, as well as QM calculations have been performed. QM/MM calculations can yield atomistic information on structure and mechanism of enzymatic reactions within the native environment of the protein,[21–30] while the QM calculations were used to investigate the transformation of the hydroxylated intermediate in water solution. As shall demonstrated, P450-catalyzed amination of the pyrrolidine derivative of lidocaine involves both the enzymatic transformation in P450 and non-enzymatic transformation in water solution.[31–34] The enzymatic transformation involves the exclusive hydroxylation of the C–H bond of the pyrrolidine derivative of lidocaine, while the following dehydration and C–N coupling reactions are found to be much favoured in aqueous situation than that in the non-polar protein environment.

2. Computational strategies and methods

2.1. Setup of the QM/MM system

Our system focuses on the RP/FV/EV variants containing R47L/Y51F/I401P/F87V/E267V mutations. The initial structure of the enzyme–substrate complex was prepared on the basis of the determined X-ray structure of $P450_{BM3}$ heam domain in complex with DMSO[35] (PDB code: 2J1M, with a resolution of 1.70 Å). Our setup is based on chain A, in which Zn ions are deleted since they are not necessary cofactors for $P450_{BM3}$. The experimental substrate, the pyrrolidine derivative of lidocaine, was docked into the active site performed with the Rosetta ligand docking.[36] According to the total energy, the top 20 docking conformations from 3000 docking results were selected for analysis. Among these 20 conformations, we found 12 of them have similar binding conformation for the substrate, in which the C3 site of the substrate and the **Cpd I**–O maintain a distance of 3.95–5.57 Å. Finally, we choose the conformation with the shortest distance (3.95 Å) to carry on the subsequent MD simulations. We assigned the protonation states of titratable residues (His, Glu, Asp) on the basis of pK_a values from the PROPKA software[37] in combination with careful visual inspection of local hydrogen-bonded networks. The histidine residues His92, His100, His138, His236, His266, His285, His361, His420 were protonated at the δ position, while His116, His171, His388, His408, His426 were protonated at the ε position. The glutamic acid residue Glu409 was protonated and all aspartic acid residues were deprotonated. For comparison, we also did MD simulation on Glu409-deprotonated state. Our MD simulations show that the binding conformation of the substrate are similar in both protonated and deprotonated cases, suggesting that the protonation state of Glu409 will not have significant impact on the BM3-mediated substrate oxidation (Fig. S2†). The force field for the **Cpd I** was parametrized using the "MCPB.py" modelling tool[38,39] of AmberTools18.[40] The Amber ff14SB force field[41] was employed for the protein residues. The general AMBER force field (GAFF)[42] was used for substrates, while the partial atomic charges were obtained from the RESP method,[43] using the B3LYP/6-31G* level of theory. Sodium ions were added to the protein surface to neutralize the total charge of the systems. Finally, the resulting system was solvated in rectangular box of TIP3P waters extending up to minimum distance of 16 Å from the protein surface.

2.2. Classical MD simulation

After a proper setup, the whole system was fully minimized using combined steepest descent and conjugate gradient methods. Then, the system was gently annealed from 10 to 300 K under a canonical ensemble for 50 ps. To achieve a uniform density after heating dynamics, 1 ns of density equilibration was performed under the NPT ensemble at the target temperature of 300 K and target pressure of 1.0 atm. Afterward, the system was further equilibrated for 4 ns under the NPT ensemble to get a well-settled pressure and temperature. Finally, a productive MD simulation under the NPT ensemble was conducted for 150 ns for the enzyme system. All MD simulations were performed with the GPU version of the Amber 18 package.[40]

2.3. QM/MM methodology

All QM/MM calculations were performed using ChemShell,[44,45] combining Turbomole[46] for the QM region and DL_POLY[47] for the MM region. The electronic embedding scheme[48] was used to account for the polarizing effect of the enzyme environment on

the QM region. Hydrogen link atoms with the charge-shift model[49] were applied to treat the QM/MM boundary. The QM subsystem is composed of the **Cpd I** moiety, its axial cysteine ligand Cys400, and the substrate. The whole QM region contains 116 atoms, which has the total charge of 0. The QM region was studied with the hybrid UB3LYP[50–52] density functional with two levels of theory. For geometry optimization, the double-ζ basis set def2-SVP,[53] labelled as B1, were used. The energies were further corrected with the larger basis set def2-TZVP[53] for all atoms, labelled as B2. Dispersion corrections computed with Grimme's D3 method[54–56] were included in all QM calculations. All the transition states (TSs) were located by relaxed potential energy surface (PES) scans followed by full TS optimizations using the dimer optimizer implemented in the DL-FIND code.[57] For comparison, we also scanned the energy barrier of H-abstraction at the larger basis set def2-TZVP directly. Our calculations show that B3LYP/def2-TZVP yields the comparable barrier for H-abstraction ($\Delta E^{\ddagger}$ = 17.9 kcal without ZPE, see Fig. S4†) as B3LYP/def2-SVP//def2-TZVP ($\Delta E^{\ddagger}$ = 18.7 kcal without ZPE). All these indicate our selected basis sets are quite reliable.

B3LYP has already been proven to be a successful[25,26,29,31,58–68] functional for studying iron-based metalloenzymes. The benchmark study of H-abstraction by an iron-oxo species found UB3LYP was the best functional for such systems.[69] All QM/MM calculations focus on the doublet state, since both the doublet and quartet states are almost degenerate and show similar reactivities in HAA reactions.

2.4. The QM calculations

All QM calculations were performed with the Gaussian 16 software package.[70] The geometries of all the TSs, reactants and intermediates involved in the reaction were fully optimized using the SMD continuum solvation model[71] at the B3LYP/6-31G(d) level of theory. Harmonic frequency calculations were performed using the equilibrium geometries to confirm the existence of first-order saddle points and local minima on the potential energy surfaces and to estimate the zero-point energies, as well as the thermal and entropic corrections. The connections between the stable structures and the transition states were ascertained by analysing the corresponding imaginary frequency modes, as well as by limited intrinsic reaction coordinate (IRC) calculations. The energies of the B3LYP/6-31G(d)-optimized structures were further refined by single-point calculations at the BMK/6-311++G(d,p) level.

3. Results and discussion

3.1. Substrate binding in the active site of the P450 variant

The substrate was first docked into the active site of variant $P450_{BM3}$ R47L/Y51F/I401P/F87V/E267V, which was found to have the highest activity.[14] Fig. 1a shows the MD equilibrated active structure of the **Cpd I** of $P450_{BM3}$ variants RP/FV/EV in complex with substrate, while Fig. 1b presents the distance fluctuations between **Cpd I**–O and the H_1 atom, the H_2 atoms of the substrate throughout the MD trajectory. It is seen that the

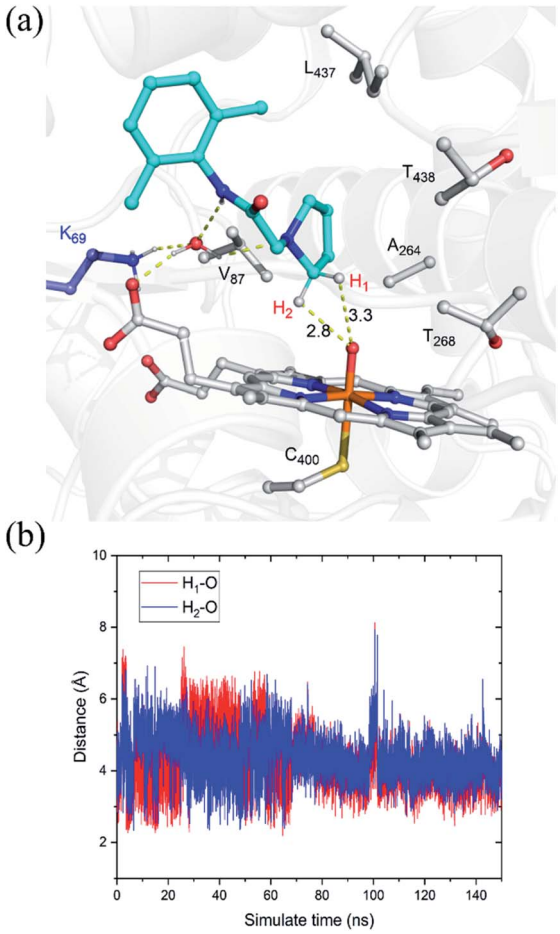

Fig. 1 (a) QM(UB3LYP/B1)/MM optimized structure of the **Cpd I** with the bound substrate, pyrrolidine derivative of lidocaine, taken from a representative snapshot in the equilibrated MD trajectory. Key distances are given in angstroms. Most hydrogen atoms of C–H bonds have been omitted for clarity. (b) Distance fluctuations between **Cpd I**–O and the H_1 atom (red), the H_2 atom (blue) of the substrate throughout the MD trajectory.

substrate maintains a relatively stable conformation in the active site, with its H_1 and H_2 atoms being both close to the O atom of **Cpd I** (Fig. 1b and S1†). In addition, we found that Lys69 forms stable hydrogen-bonding networks with the two N atoms of substrate, suggesting Lys69 is key for controlling the stability and the binding conformation of the substrate. In addition to hydrogen-bonding interactions from Lys69, the substrate is also stabilized by hydrophobic interactions with Val87, Thr327, Val267, Thr268, Leu437 and Thr438. Notably, the site mutation of F87A is found to reduce steric hindrance, enabling the substrate to approach **Cpd I**, while E267V is expected to increase the hydrophobic interaction with the substrate, thus enhancing the binding affinity of the substrate.

3.2. QM/MM and QM studies on the amination of the pyrrolidine derivative of lidocaine

3.2.1. QM/MM study on the hydroxylation of the pyrrolidine derivative of lidocaine. Fig. 2 shows the QM/MM calculated relative energy profile for the hydroxylation of the substrate by

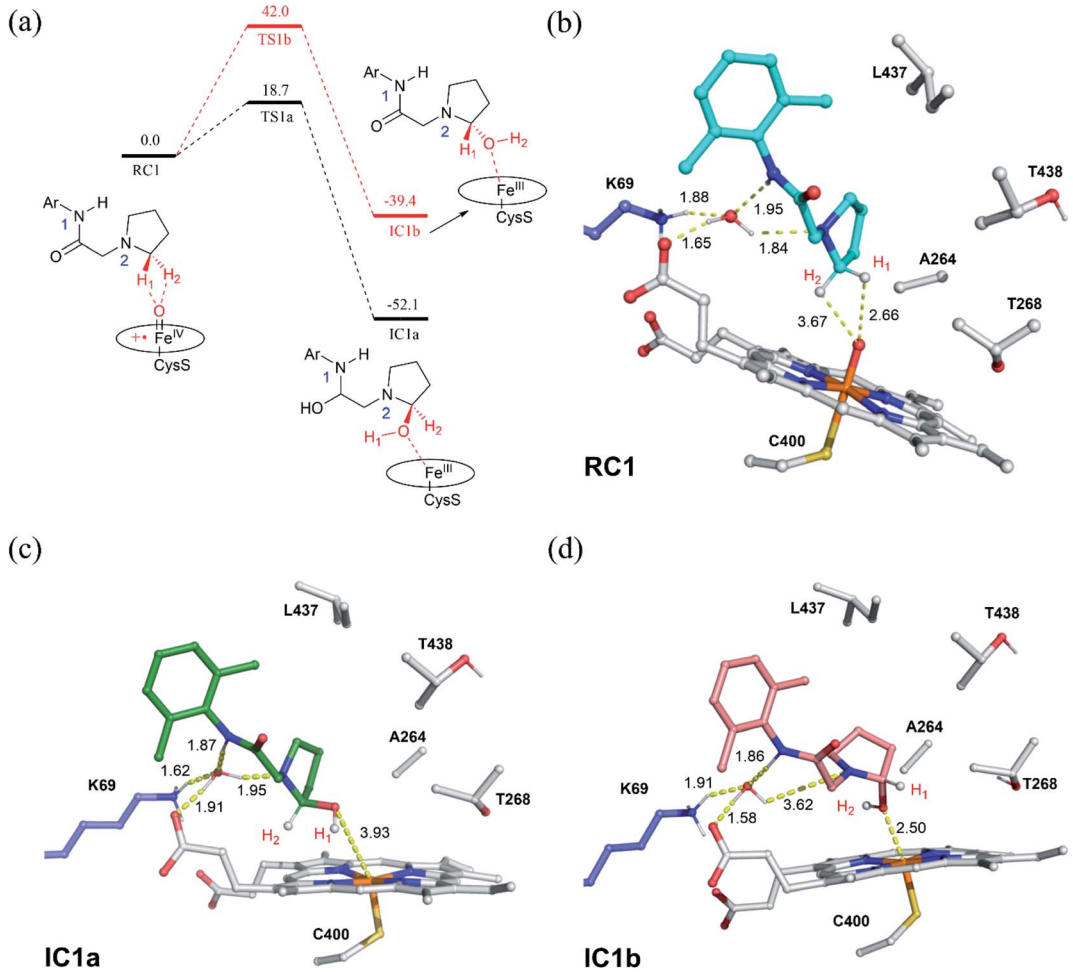

Fig. 2 (a) QM(UB3LYP/B2)/MM relative energies (kcal mol^{-1}) for the hydroxylation of the pyrrolidine derivative of lidocaine by the P450 variant. Key intermediates along the reaction energy profile are schematically drawn. (b) QM/MM optimized structures for the reactant complexes of **Cpd I**/substrate (RC1). (c) The *R*-chirality hydroxylated intermediate (IC1a) and (d) the *S*-chirality hydroxylated.

the P450$_{BM3}$ variant. In the QM/MM-optimized reactant cluster (RC1), it is seen that pro-*R* (H_1) and pro-*S* (H_2) H atoms maintain 2.66 Å and 3.67 Å with the oxo of **Cpd I**, respectively, suggesting that pro-*R* C–H bond will be selectively oxidized into the pro-*R* product. Indeed, our QM/MM calculations show that H-abstraction from pro-*R* C–H bond experiences a moderate barrier of 18.7 kcal mol^{-1}, which is much favored over that from the pro-*S* C–H bond (with a high barrier of 42.0 kcal mol^{-1}). This huge difference may be due to the significant structural changes in TS1a compared to RC1. Interestingly, our QM/MM scanning shows that the nascent substrate radical is unstable, which readily couples with the OH moiety to generate the hydroxylated intermediate (IC1a). We also investigated the H-abstraction in the quartet state, in which the reaction has a slightly higher barrier of 19.3 kcal mol^{-1} (Fig. S3†). Notably, we cannot locate the iminium intermediate in the Fe(IV)–OH/substrate radical complex, suggesting the single electron transfer process is unfavorable thermodynamically in the quartet state. Starting from the structure of the Fe(IV)–OH/substrate radical complex in the quartet state, we also re-optimized it in the doublet state and found that Fe(IV)–OH/substrate radical complex would evolve directly to the hydroxylated product. Therefore, we rule out the single electron transfer mechanism (mechanism I) in the enzymatic reactions. We assume the hydroxylated intermediate would diffuse out of the active site, since the solvation free energy of the hydroxylated intermediate (−5.54 kcal mol^{-1}) is much higher than that of the initial substrate (−1.85 kcal mol^{-1}). In addition, the bulk solvation effect of water may well stabilize a zwitterionic intermediate during cyclization (*vide infra*).

3.2.2. Cyclization of the hydroxylated intermediate in water. QM model calculations were carried out to investigate the possible conversion of hydroxylated intermediate in water solution. As shown in Fig. 3a, a well intramolecular hydrogen bond has been formed between –OH group and –NH moiety in hydroxylated intermediate (RC3). For comparison, we also optimized another isomer of RC3, in which the intermolecular H-bond is disrupted (RC3′ in Fig. S5†). However, the energy of RC3′ is 3.6 kcal mol^{-1} higher than RC3. Firstly, we investigated the dehydration of the hydroxylated intermediate in water solution. It is seen that the dehydration reaction *via* TS3a in aqueous solution has a moderate barrier of 17.5 kcal mol^{-1}.

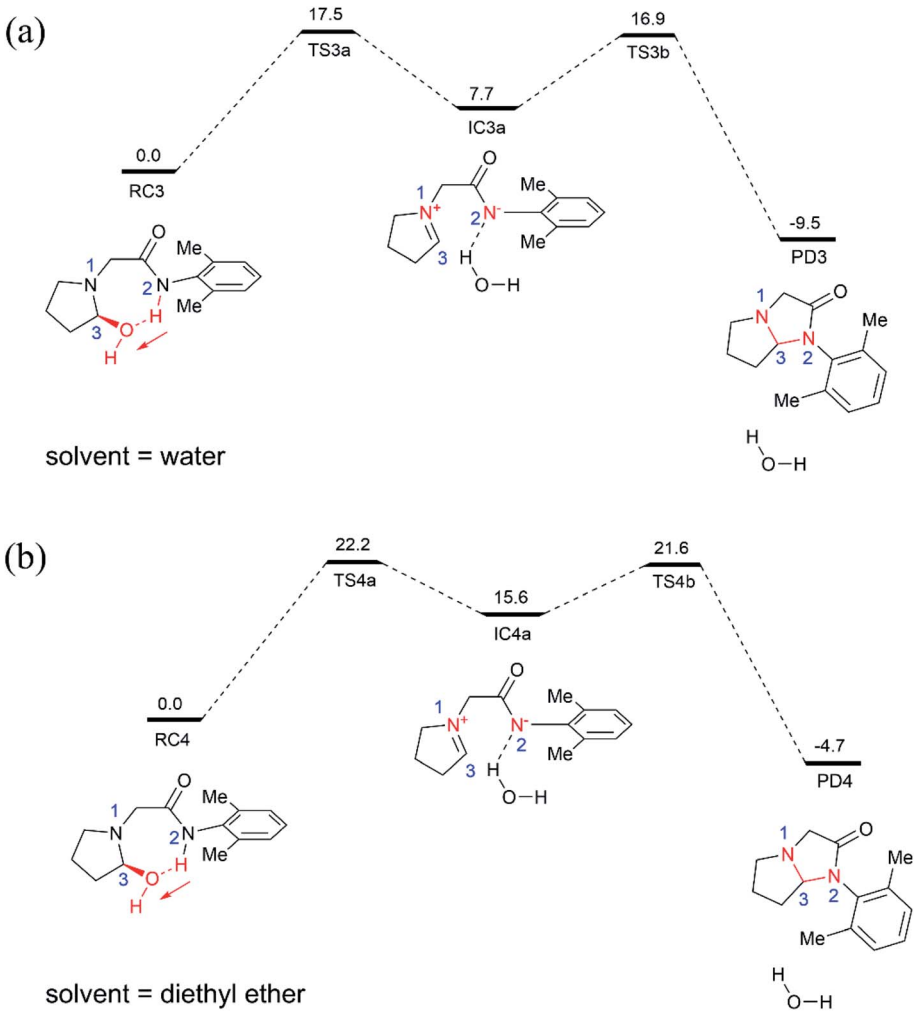

Fig. 3 BMK/6-311++G(d,p) relative Gibbs energies (in kcal mol^{-1}) for the cyclization of the hydroxylated intermediate in water (a) and diethyl ether (b) solution, shown along with schematic drawings of key intermediates along the reaction pathway. The red arrows highlight the direction of proton transfer.

This reaction leads to zwitterionic intermediate of IC3a, which lies 7.7 kcal mol^{-1} higher than RC3 species. Starting from IC3a, the intramolecular C3–N2 coupling *via* TS3b affords the product of the imidazolidine-4-ones (PD3) directly. This step experiences a small barrier of 9.2 kcal mol^{-1} (IC3a → TS3b). Clearly, the cyclization of the hydroxylated intermediate in water solution is relatively facile.

For comparison, we also examined the cyclization of the hydroxylated intermediate in diethyl ether solution (Fig. 3b), which has a dielectric constant of 4.2 and thus can mimic the hydrophobic nonpolar environment of active site of enzyme pocket. As shown in Fig. 3b, the overall cyclization reaction requires a high free energy barrier of 22.2 kcal mol^{-1}. Notably, the zwitterion intermediate (IC4a) generated in diethyl ether solution is quite unstable, 15.6 kcal mol^{-1} higher than the corresponding reactant species (RC4), suggesting that highly polar water solvent can stabilize the intermediate and speed-up the cyclization reaction.

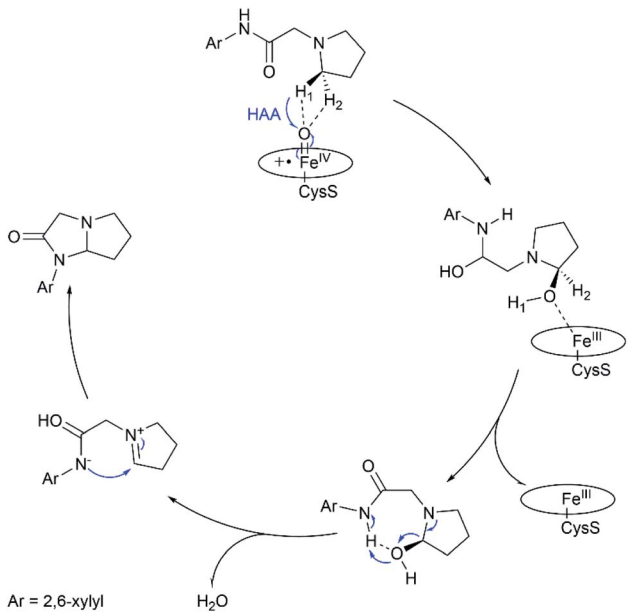

Fig. 4 Proposed catalytic mechanism for P450-catalyzed amination of the pyrrolidine derivative of lidocaine.

4. Conclusion

In summary, this work reports multi-scale calculations on the mechanistic nature of the P450-mediated amination of the pyrrolidine derivative of lidocaine. The QM/MM calculations show that the **Cpd I** active species of P450 selectively hydroxylate the C–H bond of the pyrrolidine derivatives of lidocaine and subsequent barrierless rebound of OH group leads to the hydroxylated intermediate, during which the substrate radical would be bypassed. Further QM calculations show that the hydroxylated intermediate is readily dehydrated to afford a zwitterion intermediate. Finally, a facile C–N cyclization reaction in the zwitterion intermediate generates the product of the imidazolidine-4-ones. In particular, our calculations show that the cyclization reaction is more favoured in water solution than that in the nonpolar solvent due to the stabilization effect of the polar environment on the zwitterion intermediate, suggesting that the efficient amination of the pyrrolidine derivative of lidocaine may require both the enzymatic transformation in P450 and non-enzymatic transformation in water solution. Thus, our calculations demonstrate a feasible mechanism for the 450-mediated amination of the pyrrolidine derivative of lidocaine, which could be different from other P450-catalyzed amination reactions (Fig. 4).[10,11,17,72–74]

Conflicts of interest

There are no conflicts to declare.

Acknowledgements

This work was supported by National Key Research and Development Program of China (2019YFA0906400), NSFC (No. 22073077, 21933009 and 21907082).

References

1 E. Vitaku, D. T. Smith and J. T. Njardarson, *J. Med. Chem.*, 2014, **57**, 10257–10274.
2 S. Shaik, S. Cohen, Y. Wang, H. Chen, D. Kumar and W. Thiel, *Chem. Rev.*, 2010, **110**, 949–1017.
3 D. Kumar, H. Hirao, L. Que Jr and S. Shaik, *J. Am. Chem. Soc.*, 2005, **127**, 8026–8027.
4 S. Shaik, H. Hirao and D. Kumar, *Acc. Chem. Res.*, 2007, **40**, 532–542.
5 Y. Wei, E. L. Ang and H. Zhao, *Curr. Opin. Chem. Biol.*, 2018, **43**, 1–7.
6 F. P. Guengerich, *ACS Catal.*, 2018, **8**, 10964–10976.
7 J. B. Wang, Q. Huang, W. Peng, P. Wu, D. Yu, B. Chen, B. Wang and M. T. Reetz, *J. Am. Chem. Soc.*, 2020, **142**, 2068–2073.
8 Z. Li, Y. Jiang, F. P. Guengerich, L. Ma, S. Li and W. Zhang, *J. Biol. Chem.*, 2020, **295**, 833–849.
9 T. Coleman, A. M. Kirk, R. R. Chao, M. N. Podgorski, J. S. Harbort, L. R. Churchman, J. B. Bruning, P. V. Bernhardt, J. R. Harmer, E. H. Krenske, J. J. De Voss and S. G. Bell, *ACS Catal.*, 2021, **11**, 1995–2010.
10 R. Singh, M. Bordeaux and R. Fasan, *ACS Catal.*, 2014, **4**, 546–552.
11 R. Singh, J. N. Kolev, P. A. Sutera and R. Fasan, *ACS Catal.*, 2015, **5**, 1685–1691.
12 C. K. Prier, R. K. Zhang, A. R. Buller, S. Brinkmann-Chen and F. H. Arnold, *Nat. Chem.*, 2017, **9**, 629–634.
13 X. Ren, J. A. Yorke, E. Taylor, T. Zhang, W. Zhou and L. L. Wong, *Chemistry*, 2015, **21**, 15039–15047.
14 X. K. Ren, J. A. O'Hanlon, M. Morris, J. Robertson and L. L. Wong, *ACS Catal.*, 2016, **6**, 6833–6837.
15 F. He, T. Mori, I. Morita, H. Nakamura, M. Alblova, S. Hoshino, T. Awakawa and I. Abe, *Nat. Chem. Biol.*, 2019, **15**, 1206–1213.
16 I. Morita, T. Mori, T. Mitsuhashi, S. Hoshino, Y. Taniguchi, T. Kikuchi, K. Nagae, N. Nasu, M. Fujita, T. Ohwada and I. Abe, *Angew. Chem., Int. Ed.*, 2020, **59**, 3988–3993.
17 V. Steck, J. N. Kolev, X. Ren and R. Fasan, *J. Am. Chem. Soc.*, 2020, **142**, 10343–10357.
18 V. V. Shende, Y. Khatri, S. A. Newmister, J. N. Sanders, P. Lindovska, F. Yu, T. J. Doyon, J. Kim, K. N. Houk, M. Movassaghi and D. H. Sherman, *J. Am. Chem. Soc.*, 2020, **142**, 17413–17424.
19 D. H. Scharf, P. Chankhamjon, K. Scherlach, J. Dworschak, T. Heinekamp, M. Roth, A. A. Brakhage and C. Hertweck, *Chembiochem*, 2021, **22**, 336–339.
20 I. Morita, T. Mori and I. Abe, *Chemistry*, 2021, **27**, 2963–2972.
21 A. Warshel and M. Levitt, *J. Mol. Biol.*, 1976, **103**, 227–249.
22 H. Lin and D. G. Truhlar, *Theor. Chem. Acc.*, 2006, **117**, 185–199.
23 H. M. Senn and W. Thiel, *Angew. Chem., Int. Ed.*, 2009, **48**, 1198–1229.
24 M. W. van der Kamp and A. J. Mulholland, *Biochemistry*, 2013, **52**, 2708–2728.
25 D. Kumar, W. Thiel and S. P. de Visser, *J. Am. Chem. Soc.*, 2011, **133**, 3869–3882.
26 P. Schyman, W. Lai, H. Chen, Y. Wang and S. Shaik, *J. Am. Chem. Soc.*, 2011, **133**, 7977–7984.
27 A. Warshel, *Angew. Chem., Int. Ed.*, 2014, **53**, 10020–10031.
28 B. Wang, C. Li, K. D. Dubey and S. Shaik, *J. Am. Chem. Soc.*, 2015, **137**, 7379–7390.
29 K. D. Dubey, B. Wang and S. Shaik, *J. Am. Chem. Soc.*, 2016, **138**, 837–845.
30 K. D. Dubey, B. Wang, M. Vajpai and S. Shaik, *Chem. Sci.*, 2017, **8**, 5335–5344.
31 B. J. Wang, Z. C. Cao, D. A. Sharon and S. Shaik, *ACS Catal.*, 2015, **5**, 7077–7090.
32 B. Wang, E. M. Johnston, P. Li, S. Shaik, G. J. Davies, P. H. Walton and C. Rovira, *ACS Catal.*, 2018, **8**, 1346–1351.
33 H. Zhou, B. Wang, F. Wang, X. Yu, L. Ma, A. Li and M. T. Reetz, *Angew. Chem., Int. Ed.*, 2019, **58**, 764–768.
34 L. Wang, W. Song, B. Wang, Y. Zhang, X. Xu, J. Wu, C. Gao, J. Liu, X. Chen, J. Chen and L. Liu, *ACS Catal.*, 2021, **11**, 2808–2818.
35 J. Kuper, T. S. Wong, D. Roccatano, M. Wilmanns and U. Schwaneberg, *J. Am. Chem. Soc.*, 2007, **129**, 5786–5787.
36 G. Lemmon and J. Meiler, *Methods Mol. Biol.*, 2012, **819**, 143–155.

37 C. R. Sondergaard, M. H. Olsson, M. Rostkowski and J. H. Jensen, *J. Chem. Theory Comput.*, 2011, **7**, 2284–2295.
38 P. Li and K. M. Merz Jr, *J. Chem. Inf. Model.*, 2016, **56**, 599–604.
39 P. Li and K. M. Merz Jr, *Chem. Rev.*, 2017, **117**, 1564–1686.
40 D. A. Case, I. Y. Ben-Shalom, S. R. Brozell, D. S. Cerutti, T. E. Cheatham III, V. W. D. Cruzeiro, T. A. Darden, R. E. Duke, D. Ghoreishi, M. K. Gilson, H. Gohlke, A. W. Goetz, D. Greene, R. Harris, N. Homeyer, Y. Huang, S. Izadi, A. Kovalenko, T. Kurtzman, T. S. Lee, S. LeGrand, P. Li, C. Lin, J. Liu, T. Luchko, R. Luo, D. J. Mermelstein, K. M. Merz, Y. Miao, G. Monard, C. Nguyen, H. Nguyen, I. Omelyan, A. Onufriev, F. Pan, R. Qi, D. R. Roe, A. Roitberg, C. Sagui, S. Schott-Verdugo, J. Shen, C. L. Simmerling, J. Smith, R. SalomonFerrer, J. Swails, R. C. Walker, J. Wang, H. Wei, R. M. Wolf, X. Wu, L. Xiao, D. M. York and P. A. Kollman, *AMBER 2018*, University of California, San Francisco, 2018.
41 J. A. Maier, C. Martinez, K. Kasavajhala, L. Wickstrom, K. E. Hauser and C. Simmerling, *J. Chem. Theory Comput.*, 2015, **11**, 3696–3713.
42 J. Wang, R. M. Wolf, J. W. Caldwell, P. A. Kollman and D. A. Case, *J. Comput. Chem.*, 2004, **25**, 1157–1174.
43 C. I. Bayly, P. Cieplak, W. D. Cornell and P. A. Kollman, *J. Phys. Chem.*, 1993, **97**, 10269–10280.
44 P. Sherwood, A. H. de Vries, M. F. Guest, G. Schreckenbach, C. R. A. Catlow, S. A. French, A. A. Sokol, S. T. Bromley, W. Thiel, A. J. Turner, S. Billeter, F. Terstegen, S. Thiel, J. Kendrick, S. C. Rogers, J. Casci, M. Watson, F. King, E. Karlsen, M. Sjovoll, A. Fahmi, A. Schafer and C. Lennartz, *J. Mol. Struct.: THEOCHEM*, 2003, **632**, 1–28.
45 S. Metz, J. Kastner, A. A. Sokol, T. W. Keal and P. Sherwood, *Wiley Interdiscip. Rev.: Comput. Mol. Sci.*, 2014, **4**, 101–110.
46 R. Ahlrichs, M. Bar, M. Haser, H. Horn and C. Kolmel, *Chem. Phys. Lett.*, 1989, **162**, 165–169.
47 W. Smith and T. R. Forester, *J. Mol. Graphics*, 1996, **14**, 136–141.
48 D. Bakowies and W. Thiel, *J. Phys. Chem.*, 1996, **100**, 10580–10594.
49 A. H. de Vries, P. Sherwood, S. J. Collins, A. M. Rigby, M. Rigutto and G. J. Kramer, *J. Phys. Chem. B*, 1999, **103**, 6133–6141.
50 C. T. Lee, W. T. Yang and R. G. Parr, *Phys. Rev. B: Condens. Matter Mater. Phys.*, 1988, **37**, 785–789.
51 A. D. Becke, *J. Chem. Phys.*, 1992, **97**, 9173–9177.
52 A. D. Becke, *J. Chem. Phys.*, 1993, **98**, 5648–5652.
53 F. Weigend and R. Ahlrichs, *Phys. Chem. Chem. Phys.*, 2005, **7**, 3297–3305.
54 S. Grimme, *J. Comput. Chem.*, 2006, **27**, 1787–1799.
55 S. Grimme, J. Antony, S. Ehrlich and H. Krieg, *J. Chem. Phys.*, 2010, **132**, 154104.
56 S. Grimme, S. Ehrlich and L. Goerigk, *J. Comput. Chem.*, 2011, **32**, 1456–1465.
57 J. Kastner, J. M. Carr, T. W. Keal, W. Thiel, A. Wander and P. Sherwood, *J. Phys. Chem. A*, 2009, **113**, 11856–11865.
58 H. Liu, J. Llano and J. W. Gauld, *J. Phys. Chem. B*, 2009, **113**, 4887–4898.
59 M. G. Quesne, R. Latifi, L. E. Gonzalez-Ovalle, D. Kumar and S. P. de Visser, *Chemistry*, 2014, **20**, 435–446.
60 B. Wang, D. Usharani, C. Li and S. Shaik, *J. Am. Chem. Soc.*, 2014, **136**, 13895–13901.
61 H. M. Senn, J. Kastner, J. Breidung and W. Thiel, *Can. J. Chem.*, 2009, **87**, 1322–1337.
62 K. Sen and J. C. Hackett, *J. Am. Chem. Soc.*, 2010, **132**, 10293–10305.
63 R. Lonsdale, K. T. Houghton, J. Zurek, C. M. Bathelt, N. Foloppe, M. J. de Groot, J. N. Harvey and A. J. Mulholland, *J. Am. Chem. Soc.*, 2013, **135**, 8001–8015.
64 E. Salanouve, G. Bouzemame, S. Blanchard, E. Derat, M. Desage-El Murr and L. Fensterbank, *Chemistry*, 2014, **20**, 4754–4761.
65 X. Song, J. Lu and W. Lai, *Phys. Chem. Chem. Phys.*, 2017, **19**, 20188–20197.
66 K. Bian, S. A. P. Lenz, Q. Tang, F. Chen, R. Qi, M. Jost, C. L. Drennan, J. M. Essigmann, S. D. Wetmore and D. Li, *Nucleic Acids Res.*, 2019, **47**, 5522–5529.
67 C. Hui, W. Singh, D. Quinn, C. Li, T. S. Moody and M. Huang, *Phys. Chem. Chem. Phys.*, 2020, **22**, 21696–21706.
68 S. A. Lenz, D. Li and S. D. Wetmore, *DNA Repair*, 2020, **96**, 102944.
69 R. Ramanan, K. D. Dubey, B. Wang, D. Mandal and S. Shaik, *J. Am. Chem. Soc.*, 2016, **138**, 6786–6797.
70 M. J. Frisch, G. W. Trucks, H. B. Schlegel, G. E. Scuseria, M. A. Robb, J. R. Cheeseman, G. Scalmani, V. Barone, G. A. Petersson, H. Nakatsuji, X. Li, M. Caricato, A. V. Marenich, J. Bloino, B. G. Janesko, R. Gomperts, B. Mennucci, H. P. Hratchian, J. V. Ortiz, A. F. Izmaylov, J. L. Sonnenberg, D. Williams-Young, F. Ding, F. Lipparini, F. Egidi, J. Goings, B. Peng, A. Petrone, T. Henderson, D. Ranasinghe, V. G. Zakrzewski, J. Gao, N. Rega, G. Zheng, W. Liang, M. Hada, M. Ehara, K. Toyota, R. Fukuda, J. Hasegawa, M. Ishida, T. Nakajima, Y. Honda, O. Kitao, H. Nakai, T. Vreven, K. Throssell, J. A. Montgomery Jr, J. E. Peralta, F. Ogliaro, M. J. Bearpark, J. J. Heyd, E. N. Brothers, K. N. Kudin, V. N. Staroverov, T. A. Keith, R. Kobayashi, J. Normand, K. Raghavachari, A. P. Rendell, J. C. Burant, S. S. Iyengar, J. Tomasi, M. Cossi, J. M. Millam, M. Klene, C. Adamo, R. Cammi, J. W. Ochterski, R. L. Martin, K. Morokuma, O. Farkas, J. B. Foresman and D. J. Fox, *Gaussian 16, Revision B.01*, Wallingford CT, 2016.
71 A. V. Marenich, C. J. Cramer and D. G. Truhlar, *J. Phys. Chem. B*, 2009, **113**, 6378–6396.
72 Z. Li, D. J. Burnell and R. J. Boyd, *J. Phys. Chem. B*, 2017, **121**, 10859–10868.
73 Z. J. Jia, S. Gao and F. H. Arnold, *J. Am. Chem. Soc.*, 2020, **142**, 10279–10283.
74 Z. Fu, L. Yang, D. Sun, Z. Qu, Y. Zhao, J. Gao and Y. Wang, *Dalton Trans.*, 2020, **49**, 11099–11107.